# Stratum corneum model membranes : molecular organization in relation to skin barrier function

Groen, D.

# Chapter 5

## Model membranes prepared with ceramide EOS, cholesterol and free fatty acids form a very unique lamellar phase

Daniël Groen, Gerrit S. Gooris, Joke A. Bouwstra

*Langmuir*, vol. 26, no. 6, pp. 4168-75.

## Abstract

The lipid matrix present in the human stratum corneum (the thin, uppermost layer of the skin) is considered to play a crucial role in the skin barrier function. The lipid matrix consists of ceramides, cholesterol and free fatty acids. The 13 nm lamellar phase present in the lipid matrix of the stratum corneum is very characteristic and plays an important role in the skin barrier function. One subclass of ceramides with a linoleic acid linked to a very long acyl (referred to as EOS) plays a crucial role in the formation of the 13 nm lamellar phase.

In this paper we focus on the lipid phase behaviour of EOS mixed with cholesterol or with cholesterol and free fatty acids. Our studies reveal that an equimolar ratio of EOS, cholesterol and free fatty acids forms a lamellar phase with a very long repeat distance of approximately 14.7 nm. This phase has an exceptional behaviour as in the thermotropic response the fatty acid chains and the ceramide chains undergo an order-disorder transition at different temperature ranges, while a part of the hydrocarbon chains of ceramides and fatty acids are mixing in the orthorhombic lattice. Based on these observations a molecular model for the 14.7 nm phase has been proposed, in which the lipids are organised in a lamellar phase with three different lipid layers in a symmetric unit cell.

## Introduction

The natural function of the skin is to protect the body from unwanted influences of the environment and to prevent the body from desiccation. The main barrier for diffusion of substances across the skin is the outermost layer of the skin, the stratum corneum (2). The stratum corneum is a transparent thin layer of around 15 µm in thickness and consists of hydrophilic corneocytes embedded in lipid regions. The structure of the stratum corneum is often compared to a brick wall, in which the corneocytes form the bricks and the lipids form the mortar. The corneocytes are surrounded by a densely crosslinked protein layer, the cornified envelope. A monolayer of lipids is chemically linked to the cornified envelope and forms the link between the hydrophilic corneocytes and the hydrophobic lipids, which are the major constituents in the intercellular regions (3). As the lipid located in the intercellular regions form the only continuous structure in the stratum corneum, substances always have to cross the intercellular lipid regions before entering the viable epidermis underneath the stratum corneum (4, 5). For this reason the lipid composition and organisation is always considered to play a crucial role in the skin barrier function. The main lipid classes in stratum corneum are ceramides (CERs), cholesterol (CHOL) and free fatty acids (FFAs) in an approximately equal molar ratio (6-8). The lipids form two crystalline lamellar phases with repeat distances of approximately 6 and 13 nm (9-14). The 13 nm lamellar phase is very characteristic for the structure and is considered to be very important for the skin barrier function. When using human stratum corneum, only one group did not report the 13 nm lamellar phase (15). In that publication the set-up of the X-ray beam precluded the detection of reflections corresponding to long spacings and therefore no LPP was reported. The lateral packing of the lipids in the lipid lamellae is mainly orthorhombic, although the hexagonal lateral packing is also formed (10, 16-19). In human stratum corneum at least 11 subclasses of CERs are identified (8). The most important CERs are classified according to their base, which is either a sphingoid base (S), phytosphingoid base (P), or 6 hydroxy sphingoid base (H). Among these

CERs, there are 3 CER subclasses having a very exceptional molecular architecture, referred to as acylCERs (8, 20). The acylCERs have a linoleic acid ester linked to a ω-hydroxy fatty acyl chain with a length of approximately 32 carbon atoms, see Figure 1 (7). Furthermore, the FFAs are mainly saturated having a predominant chain length of 24 to 26 carbon atoms (21). Previous studies using mixtures based on either isolated CERs or synthetic CERs showed that these lipid mixtures resemble very closely the lipid organisation in human stratum corneum (22-24). This simplified synthetic CER mixture consists of one acylceramide (EOS) and 4 other CER subclasses with either a sphingosine or a phytosphingosine base. Using these CER subclasses, mixed with CHOL and FFAs, it was demonstrated that EOS, see Figure 1, is very important for the formation of the 13 nm lamellar phase (24, 25). In additional studies it was observed that the linoleate moiety of the acylCER is in a pseudofluid phase, and that the presence of this pseudofluid phase is also crucial for the formation of the 13 nm lamellar phase (23, 26). When we reduced the number of CERs by selecting only sphingosine-based, phytosphingosine-based or α-hydroxy-based ceramides, it was still possible to form the long periodicity phase (26). However, the composition of the selected CER mixtures affected the lateral packing of the lipids as far as the formation of the orthorhombic phase is concerned.

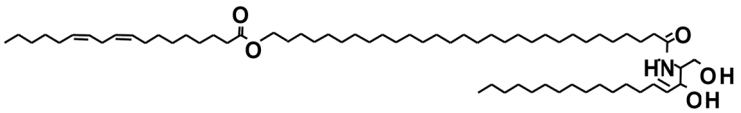


**Figure 1: Molecular structure of the most abundant EOS. The nomenclature is according to Motta et al. (1).**

In addition several studies were performed on the phase behaviour of single CERs mixed with a single FFA and/or CHOL. Although the lateral packing of these mixtures is often very similar to that observed in stratum corneum, the lamellar phase behaviour and the mixing properties between CERs and FFA are different (27-31).

As EOS plays a crucial role in the formation of the 13 nm lamellar phase, the current study is focussed on the phase behaviour of EOS combined with either only CHOL or with CHOL and FFA. The central questions we wanted to answer in this study are: 1) Is it possible for EOS in a mixture with FFA and CHOL to form the LPP in the absence of the other CER subclasses? and 2) What is the molecular organisation of the phases formed in the equimolar EOS:CHOL:FFA mixture? Our studies reveal that EOS:CHOL:FFA mixtures form a very exceptional lamellar phase that is different from the 13 nm lamellar phase observed in the stratum corneum.

## Material and Methods

### Materials

Synthetic EOS with an ω-hydroxy chain length of 30 or 27 carbon atoms (deuterated linoleate, referred to as dEOS) was generously provided by Cosmoferm B.V. (Delft, The Netherlands). Palmitic acid (C16:0), stearic acid (C18:0), arachidic acid (C20:0), behenic acid (C22:0), tricosanoic acid (C23:0), lignoceric acid (C24:0), cerotic acid (C26:0), cholesterol and acetate buffer salts were purchased from Sigma-Aldrich Chemie GmbH (Schnelldorf, Germany). All organic solvents used are of analytical grade and manufactured by Labscan Ltd. (Dublin, Ireland). The water used is of Millipore quality.

Perdeuterated FFAs (referred to as DFFAs) with a chain length of C16:0 and C22:0 were obtained from Larodan ( Malmö, Sweden). The DFFA with chain length of C18:0 and C20:0 were purchased from Cambridge Isotope laboratories (Andover, Massachusetts), while DFFA with a chain length of C24:0 was obtained from ARC laboratories (Apeldoorn, The Netherlands).

### Preparation of the lipid mixtures

For the free fatty acids mixture FFA7, the following composition was selected: C16:0, C18:0, C20:0, C22:0, C23:0, C24:0 and C26:0 at molar ratios of 1.8, 4.0, 7.7, 42.6, 5.2, 34.7 and 4.1 respectively. This chain length distribution is based on a FFA composition in SC (32). For FTIR studies, the protonated FFA7 were replaced by protonated FFA5 or deuterated DFFA5 using a slightly different FFA composition, namely C16, C18, C20, C22 and C24 at molar ratios of 1.8, 4.0, 7.6, 47.8 and 38.8 respectively, as not all the FFA were available in the deuterated version. SAXD measurements of mixtures with FFA5 or DFFA5 demonstrated that these mixtures form the same lamellar phases (data not shown).

EOS, dEOS, CHOL, FFA7 or FFA5 or DFFA5 were dissolved in chloroform:methanol (2:1 v/v). The solvents were mixed in appropriate ratios to achieve the required compositions. About 1.5 mg of lipids in solution was sprayed in the centre of a mica strip of 10 x 2 mm (X-ray diffraction studies) or on an AgBr window in 10 x 10 mm area (FTIR studies) using a Camag Linomat IV sample applicator (Muttenz, Switzerland). Spraying was performed at a rate of 5 µl/min, under a gentle stream of nitrogen gas. Subsequently, each lipid sample was equilibrated at a temperature around the melting point of the lipid mixture, which was either 70 or 80°C dependent on the composition of the mixture. After 10 minutes of equilibration close to the melting temperature range, the sample was cooled down to room temperature.

### X-ray diffraction analysis

All samples were measured at the European Synchrotron Radiation Facility (ESRF) in Grenoble (France), at the small-angle X-ray diffraction (SAXD) beam line BM26b. The lipid samples were inserted into a temperature controlled sample holder with two mica windows. Diffraction data were collected on a two-dimensional multi-wire gas-filled area detector with 512×512 pixels of 0.25 mm spatial resolution. The spatial calibration of this detector was performed using silver behenate (d = 5.838 nm). Data

acquisition was performed for a period of 10 to 15 min. The scattered intensities were measured as a function of θ, the scattering angle. From the scattering angle the scattering vector (q) was calculated by $q = 4\pi\sin\theta/\lambda$, in which λ is the wavelength at the sample position. One dimensional intensity profiles were obtained by transformation of the two dimensional SAXD pattern from Cartesian (x,y) to polar (ρ,φ) coordinates and subsequently, integration over φ from 60 to 120 degrees. These diffraction curves were plotted as a function of q ($nm^{-1}$), the scattering vector in reciprocal space. The positions of the diffraction peaks are identified by their spacing, which is $2\pi/qn$, in which qn is the position of the diffraction peak of order n. The repeat distance of a lamellar phase is calculated from the spacings of the various orders of the diffraction peaks attributed to that phase, namely $d=2n\pi/qn$. When examined as function of temperature, the acquisition time for each sequential measurement was 3 minutes and the heating rate was 1ºC/min.

## FTIR analysis

All spectra were acquired on a BIORAD FTS4000 FTIR spectrometer (Cambridge, Massachusetts) equipped with a broad-band mercury cadmium telluride detector, cooled with liquid nitrogen. The sample cell was closed by a second AgBr window. The sample was under continuous dry air purge starting 1 hour before the data acquisition. The spectra were collected in transmission mode, as a co-addition of 256 scans at 1 cm-¹ resolution during 4 minutes. In order to detect the phase transition the sample temperature was increased at a heating rate of 0.25˚C/min resulting in 1°C temperature raise during each measurement. The lipid phase behavior was examined between 20˚C and 100˚C. The software used was Win-IR pro 3.0 from Biorad (Cambridge, Massachusetts). The spectra were deconvoluted using a half-width of 4 $cm^{-1}$ and an enhancement factor of 1.7.

## Results

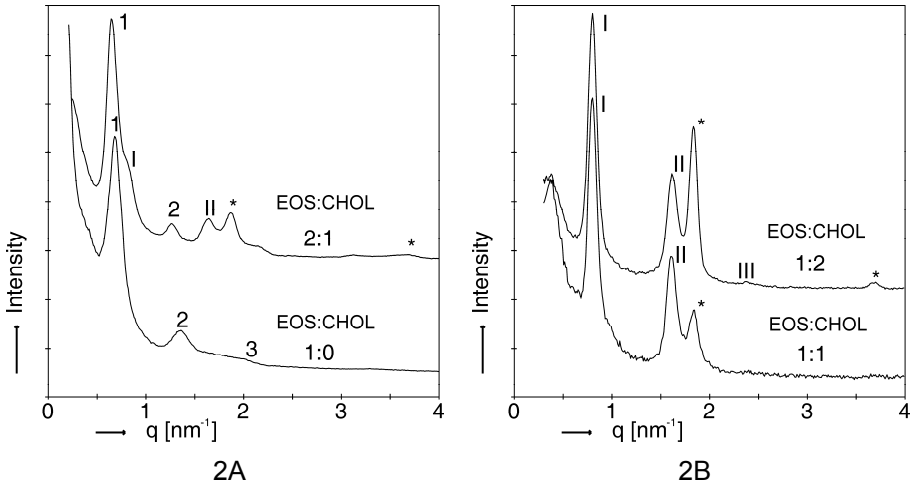


**Figure 2: X-ray diffraction patterns of mixtures with EOS:CHOL in different molar ratios. The diffraction peaks indicated by Arabic numbers (1 to 3) are associated to a lamellar phase with a periodicity of approximately 9.8 nm. The peaks indicated by roman numbers (I to III) arise from a shorter lamellar phase with repeat distance of approximately 7.7 nm. The remaining peaks that are present in the diffraction patterns, indicated by asterisks, arise from crystalline cholesterol (repeat distance is 3.4 nm).**

### Phase behaviour of EOS and EOS:CHOL mixtures

The diffraction profiles of EOS and the EOS:CHOL mixtures are provided in Figure 2A and 2B. The diffraction profile of EOS is characterized by 3 reflections positioned at q= 0.68, 1.35 and 2.0 $nm^{-1}$ indicating a lamellar phase with a repeat distance of 9.3 nm. The diffraction pattern of the EOS:CHOL mixture with a molar ratio of 2:1 reveals the presence of at least three reflections (q= 0.65, 1.26 and 1.89 $nm^{-1}$) representing a lamellar phase with a repeat distance of 9.8 nm. The 3rd order peak might also partly be due to phase separated CHOL (33) indicated by reflections located at q=1.87 and 3.74 $nm^{-1}$. In addition a reflection is observed at a spacing of

3.83 nm (q= 1.63 $nm^{-1}$), of which the first order is most probably the shoulder observed at the right-hand side of the peak at q= 0.64 $nm^{-1}$ representing a phase with a repeat distance of approximately 7.7 nm. Therefore it seems that in the EOS:CHOL mixture with a 2:1 molar ratio two phases coexist: a lamellar phase with a repeat distance of 9.8 nm and another phase with a repeat distance of approximately 7.7 nm. Increasing the CHOL content to an equimolar EOS:CHOL ratio promotes the presence of the 7.7 nm phase, as is clearly depicted in Figure 2B. The reflections attributed to this phase are located at q= 0.81 and 1.62 $nm^{-1}$. Finally we increased the CHOL content to an EOS:CHOL molar ratio of 1:2. Only the 7.7 nm phase is present (q= 0.82 and 1.63 $nm^{-1}$ and a very weak reflection at q= 2.37 $nm^{-1}$) together with phase separated CHOL.

### Phase behaviour of EOS:CHOL:FFA7 mixtures

First the phase behaviour of an equimolar EOS:CHOL:FFA7 mixture was studied. As depicted in Figure 3A, a series of peaks is present that can be attributed to only one lamellar phase with a repeat distance of 14.7 nm (reflections at q= 0.42 (1st order), 0.86 (2nd), 1.28 (3rd), 1.72 (4th), 2.13 (5th), 2.99 (7th) and 3.41 (8th) $nm^{-1}$). Choosing this lipid composition a lamellar phase is formed with a longer periodicity than observed in the LPP. In addition two reflections attributed to phase separated crystalline CHOL are present. Reduction in CHOL level to an EOS:CHOL:FFA7 molar ratio of 1:0.8:1 resulted in a diffraction profile with reflections at 0.89 (1st), 1.69 (2nd) and 3.43 ( 4th) $nm^{-1}$ strongly indicating the presence of a 7.3 nm lamellar phase, see Figure 3B. An additional peak is observed at a spacing of 5.5 nm (q=1.13 $nm^{-1}$), which is attributed to another unknown phase. Reducing the CHOL content further results in the formation of a phase with a repeat distance of around 9.3 nm, very similar to the phase changes of EOS:CHOL mixtures when reducing the CHOL level (not shown). Therefore reducing the CHOL level below an equimolar ratio strongly reduces the formation of the phase with a very long repeat distance of approximately 14.7 nm. From the studies presented in Figure 2 it is clear that in the

absence of a FFA7 mixture with chain-lengths varying from 16 to 26 carbon atoms, no 14.7 nm lamellar phase is formed, while Figure 3A exhibits reflections all contributing to the 14.7 nm phase.

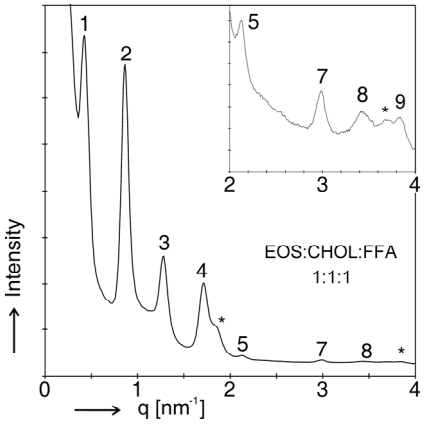


3A

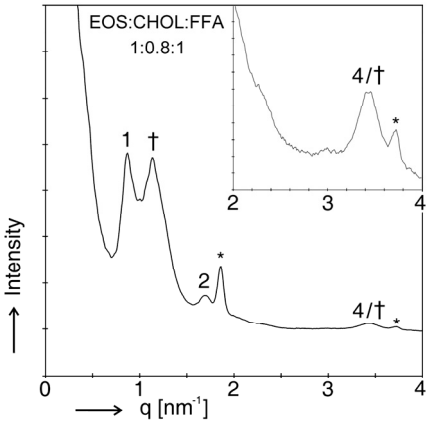


3B

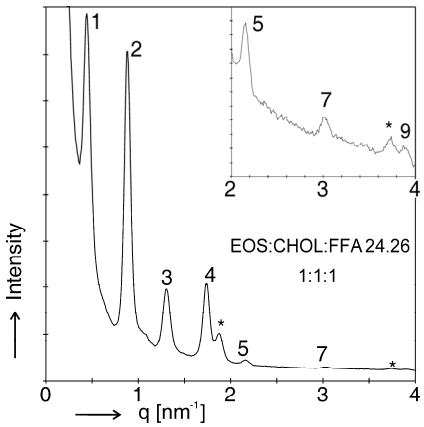


3C

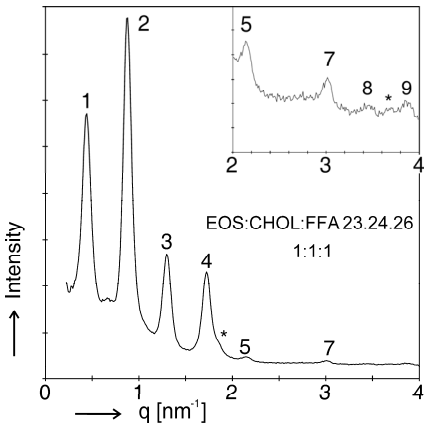


3D

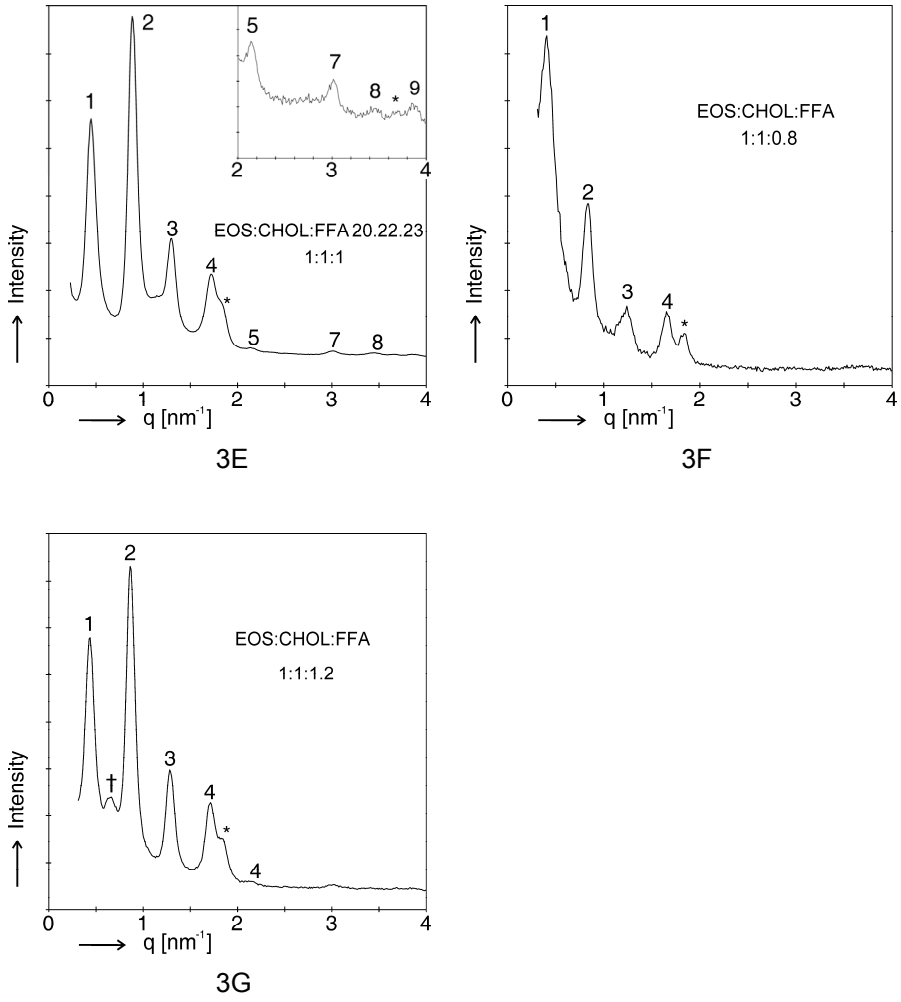


**Figure 3: X-ray diffraction patterns of EOS:CHOL:FFA in different molar ratios or with varying FFA composition. In these patterns the Arabic numbers (1 up to 9) denote the diffraction peaks that are associated to the very long periodicity phase (with a repeat distance of around 14.7 nm). If an additional phase is present in a diffraction pattern the peaks associated to this phase are indicated by a dagger (†). Diffraction peaks of crystalline cholesterol are indicated by asterisks.**

The next question to be answered is, do we need such a wide variation in chain length distribution in the FFA7 mixture or can we replace this mixture by a less complex one? In order to answer this question we reduced the number of FFA components to only three or two, in which the FFA composition was gradually changed from long chain FFA to shorter chain FFA.

In Figure 3C the diffraction profile of the equimolar EOS:CHOL:FFA24.26 mixture is depicted. (FFA24.26 indicates two fatty acids in equimolar ratio with a chain length of 24 carbon and 26 carbon atoms.) Similarly to the EOS:CHOL:FFA7 mixture 6 reflections are present, which can all be attributed to a lamellar phase with a repeat distance of 14.4 nm (positions of the reflections are at q= 0.44, 0.87, 1.29, 1.73, 2.16 and 3.00 $nm^{-1}$). The presence of crystalline CHOL in separate domains can be deduced from the peaks at 1.87 and 3.74 $nm^{-1}$. When adding a fatty acid with a chain length of 23 carbon atoms (resulting in an equimolar EOS:CHOL:FFA23.24.26 mixture) a lamellar phase with a repeat distance of 14.5 nm is formed, see Figure 3D. With a further reduction in FFA chain length, using a mixture of equimolar EOS:CHOL:FFA20.22.23, it was still possible to form a 14.4 nm lamellar phase (reflections at q= 0.44, 0.88, 1.28, 1.71 and 2.12 and 3.00 $nm^{-1}$), see Figure 3E. However, the formation of this phase was less reproducible. A further reduction in the FFA chain lengths to FFA16.18.20 did not result in the formation of a lamellar phase with a very long repeat distance (not shown). This indicates that in order to form this phase, fatty acids with a long chain are required.

If we now reduce the number of FFA to only a single FA and study the phase behaviour of EOS:CHOL:FA equimolar ratio by varying the FA chain length between 16 and 24 carbon atoms, the lamellar phase with a repeat distance of around 14.5 nm is not formed in a reproducible manner. Only occasionally this phase is formed when using FA26, FA24 and FA23 (not shown) demonstrating that a limited variation in chain length of the FFA is required to form this lamellar phase with long repeat distance in a reproducible manner.

Finally we investigated whether the level of FFA7 could be reduced or increased while still forming the lamellar phase with the long repeat distance. A reduction of the FFA7 level to an 0.8 molar ratio resulted in the formation of a lamellar phase with a long repeat distance of around 15.1 nm, see Figure 3F. When increasing the FFA7 level to an EOS:CHOL:FFA7 level of 1:1:1.2, the lamellar phase with a long repeat distance (14.4 nm) could still be formed, although a small population of lipids also forms another phase as indicated by the peak position at 0.64 $nm^{-1}$ (dagger in Figure 3G). The EOS:CHOL:FFA7 1:1:1.2 composition was also measured as function of temperature. The data is provided in Figure 4. Increasing the temperature at a heating rate of 1.5ºC/min did not change the lamellar phases until a temperature of around 66ºC was reached. At this temperature the reflections attributed to the 14.4 nm lamellar phase reduced in intensity and disappeared at approximately 74ºC, while the reflection at 0.64 $nm^{-1}$ disappeared at around 78ºC.

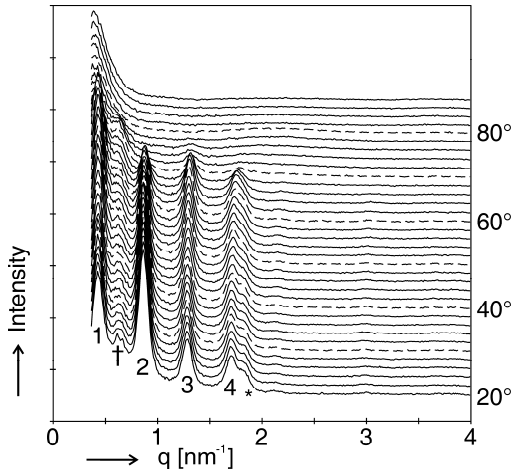


**Figure 4: The x-ray diffraction profile of EOS:CHOL:FFA7 1:1:1.2 as a function of temperature. Diffraction peaks associated to the very long lamellar phase (with a periodicity of 14.4 nm) are indicated by Arabic numbers, the additional phase by a dagger (peak position at 0.64 $nm^{-1}$) and crystalline cholesterol by an asterisk.**

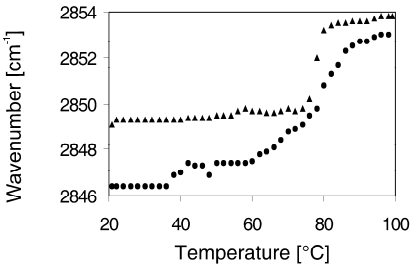
Wavenumber [cm-1]
2854
2852
2850
2848
2846
20
40
60
80
100
Temperature [°C]

5A

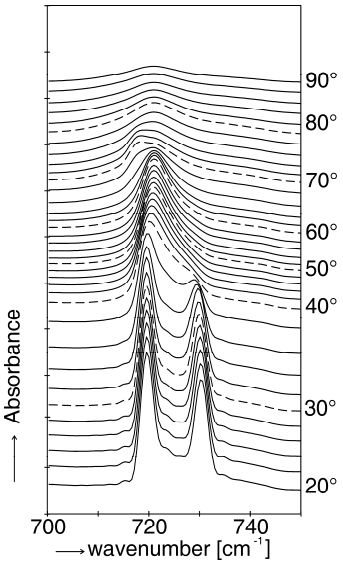
90°
80°
70°
60°
50°
40°
30°
20°
Absorbance
700
720
740
wavenumber [cm-1]

5B

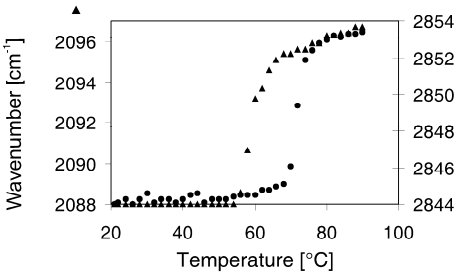
Wavenumber [cm-1]
2096
2094
2092
2090
2088
2854
2852
2850
2848
2846
2844
20
40
60
80
100
Temperature [°C]

5C

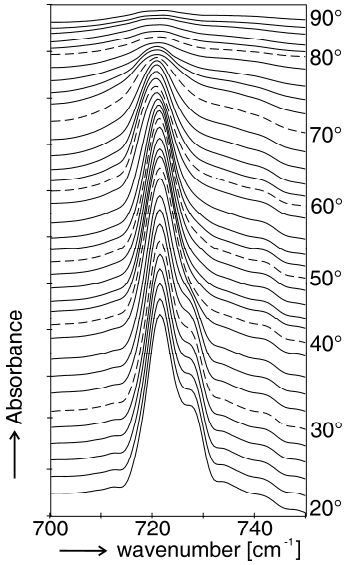
90°
80°
70°
60°
50°
40°
30°
20°
Absorbance
700
720
740
wavenumber [cm-1]

5D

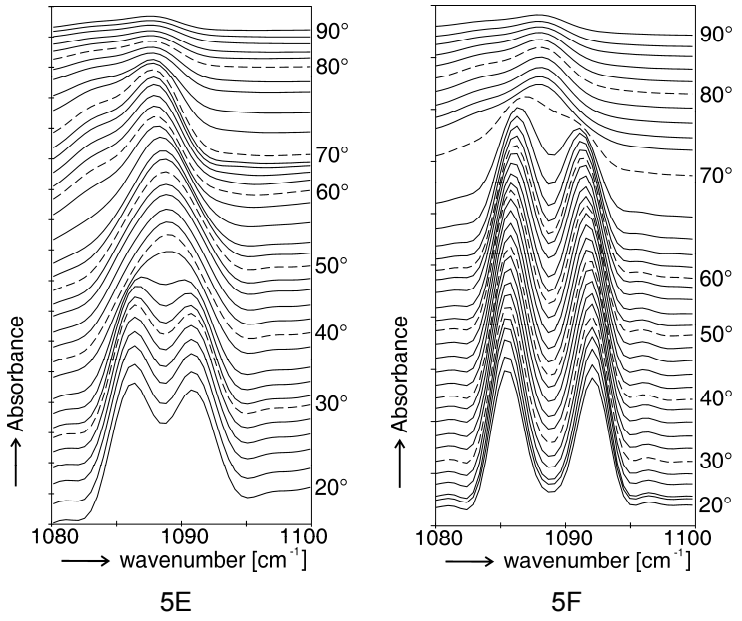


**Figure 5: FTIR spectra of EOS:CHOL:FFA5 in different ratios or with DFFA5, as a function of temperature. A) The $CH_2$ symmetric stretching peak positions of EOS:CHOL 1:1 (triangles) and EOS:CHOL:FFA5 1:1:1 (circles). B) The $CH_2$ rocking vibrations of EOS:CHOL:FFA5 1:1:1. C) The symmetric stretching peak positions of the $CH_2$ chains (circles) and $CD_2$ chains (triangles) in a mixture with EOS:CHOL:DFFA5 1:1:1. D) The $CH_2$ rocking and E) $CD_2$ scissoring vibrations of the EOS:CHOL:DFFA5 mixture. F) Scissoring vibrations from a mixture with DFFA5 only.**

## Conformational ordering and lateral packing of the equimolar EOS:CHOL mixture

The $CH_2$ symmetric stretching vibrations are a measure for the conformational ordering of the hydrocarbon chains in the mixture. The thermotropic response of the $CH_2$ symmetric stretching vibration of the equimolar EOS:CHOL mixture is provided in Figure 5A. At 20ºC the $CH_2$ symmetric stretching vibration is located at 2849.2 $cm^{-1}$. Increasing the temperature to 75ºC changes the $CH_2$ symmetric stretching vibrations only

slightly to 2849.8 $cm^{-1}$. A further increase in temperature results in large shift to a value of 2853.2 $cm^{-1}$ at 81ºC indicating an order-disorder transition in a very narrow temperature region. When focussing on the scissoring vibrations, only one peak is observed at 1467 $cm^{-1}$, demonstrating that the mixture forms a hexagonal lateral packing (not shown). Possibly a subpopulation of the lipids may also form a liquid phase (see below).

## Conformational ordering and lateral packing of the EOS:CHOL:FFA5 and EOS:CHOL:DFFA5 mixtures

To determine the thermotropic conformational ordering of the equimolar EOS:CHOL:FFA5 mixture, the $CH_2$ symmetric stretching vibrations are measured between 20 and 90ºC, see Figure 5A. At 20ºC the $CH_2$ symmetric stretching vibration is located at 2846.4 $cm^{-1}$. Upon heating no shift in the peak position of the vibration is observed until 38ºC, at which a small shift to 2847.4 $cm^{-1}$ is observed. A further increase in temperature to 60ºC does not change the $CH_2$ symmetric stretching vibrations. Above 60ºC a gradual shift to higher wave numbers is observed. The midrange temperature of this transition to a disordered phase is at around 78ºC. At 90ºC the $CH_2$ symmetric stretching vibrations are at around 2853 $cm^{-1}$, indicating conformational disordering. The $CH_2$ rocking and scissoring vibrations of the hydrocarbon chains provide information about the lateral packing of the lipids in the lamellae. The contours of the rocking vibrations in the spectrum reveal a splitting with vibrations at 719.5 $cm^{-1}$ and 730.3 $cm^{-1}$ at 20ºC, see Figure 5B. This splitting is caused by a short range coupling between the neighbouring hydrogen atoms of the hydrocarbon chains in the orthorhombic packing. As the magnitude of this splitting approaches 11 $cm^{-1}$, which is close to its maximum value, it may be concluded that large domains of this orthorhombic packing are formed. However, as the splitting is not complete, a subpopulation of lipids still forms a hexagonal lateral packing. A gradual increase in temperature results in a disappearance of the splitting between 40ºC and 42ºC. At this temperature only one peak is observed, demonstrating that the lateral packing is mainly hexagonal. These

observations have been confirmed by the scissoring frequencies located in the spectrum at 1463.1 and 1473.3 $cm^{-1}$ (not shown).

When we replace the protonated FFA5 by DFFA5 in the equimolar lipid mixture, information can be obtained on the mixing properties of the FFA and EOS on two levels. Firstly as the vibrations of the deuterated fatty acids and the protonated EOS occur at a different wavenumber, the vibrations can be measured simultaneously. For this reason it is possible to determine whether the transition from an ordered to a disordered phase for the FFA and EOS occurs in the same temperature range. Secondly, as no short range coupling occurs between protonated and deuterated chains in the orthorhombic lattice, it is possible to determine whether the protonated and deuterated lipids participate in the same orthorhombic lattice.

When examining the thermotropic response of $CH_2$ symmetric stretching vibrations, at 20ºC the maximum of the contour is located at 2844.0 $cm^{-1}$. This peak position does not shift until a temperature of around 50ºC, see Figure 5C. At that temperature a gradual increase of the wavenumber of the symmetric stretching vibrations is observed until around 68ºC. This suggests an increase in conformational disordering in a subpopulation of protonated chains. A further increase in temperature results in a steep shift in the stretching vibrations to higher wavenumber until 74ºC indicating a conformational disordering occurring in a very narrow temperature range. Above 74ºC the change in stretching frequency levels off and reaches a value of around 2853.4 $cm^{-1}$ at 90ºC. When examining the $CD_2$ symmetric stretching vibrations of the DFFA5 in the same mixture, the maximum of the $CD_2$ symmetric stretching contour is at 2088.0 $cm^{-1}$ at 20ºC. The peak position does not shift until a temperature of around 54ºC. A further increase in temperature results in a steep shift of the maximum peak position to 2095.5 $cm^{-1}$ at 66ºC indicating a conformational disordering of the FFA. A further increase in temperature results in a gradual increase in the $CD_2$ symmetric stretching frequencies to around 2096.7 $cm^{-1}$ at 90ºC. The rocking and scissoring $CH_2$ and $CD_2$ vibrations provide information on the lateral packing and mixing properties within the orthorhombic phase. These

contours are provided in Figure 5D and 5E, respectively. At 20ºC a slight splitting in the $CH_2$ rocking frequencies is observed with peak positions at 721.4 and 728.0 $cm^{-1}$. When gradually increasing the temperature, a reduction in the high wavenumber peak intensity starts at 34ºC and the splitting disappears at 38ºC. The $CH_2$ scissoring vibrations in the spectrum confirm the disappearance of the $CH_2$ short range coupling in this temperature region. The $CD_2$ scissoring contours of the EOS:CHOL:DFFA5 also clearly show a splitting of the peak positions at 20ºC. The low frequency and high frequency components are located at 1086.3 and 1090.9 $cm^{-1}$ respectively. The thermotropic behaviour of the $CD_2$ scissoring vibrations reveal a disappearance of the splitting between 36 and 40ºC. This suggests the disappearance of the orthorhombic packing. For comparison in Figure 5F, the thermotropic behaviour of single DFFA5 contours are provided. These show a splitting at 1085.6 and 1091.2 $cm^{-1}$. This splitting remains in the temperature range between 20 and 70ºC. The slopes forming the dip in between the two scissoring vibrations are much steeper than the slopes forming the dip between the low and high wavenumber of the $CD_2$ scissoring vibrations in the spectrum of the CER:CHOL:DFFA5 mixture. This shows that at least a subpopulation of DFFA is mixing with the protonated CER, but that a fraction of the DFFA chains are still able to interact and are thus located at neighbouring positions in the orthorhombic lattice.

## Conformational ordering of the linoleate moiety in the equimolar mixture of dEOS(C27):CHOL:FFA5

In order to determine whether the linoleate moiety in the equimolar mixture is in a disordered state the $CD_2$ symmetric stretching vibrations were measured of the equimolar dEOS(C27):CHOL:FFA5 mixture. In this mixture only the linoleate moiety is deuterated, which permits a selective measurement of the deuterated linoleate vibrations. The $CD_2$ stretching vibrations reveal that already at room temperature the maximum peak is close to 2099.0 $cm^{-1}$ and almost does not change in peak position until 70°C, then a weak shift occurs to 2101.2 $cm^{-1}$ which does not change until a

temperature of 90ºC is reached (not shown). This obviously shows that the unsaturated linoleate chain is already in conformational disorder at room temperature, but increases slightly in disorder at around 72ºC, which is a similar temperature range at which the lamellar phase with the long periodicity disappears.

## Discussion

The purpose of the studies described in this paper was to determine whether EOS in the absence of additional CERs is able to form the LPP. For this reason phase behaviour studies were performed with EOS, EOS:CHOL and EOS:CHOL:FFA mixtures. Our studies reveal that only in EOS:CHOL:FFA mixtures a lamellar phase with a very long periodicity of 14.7 nm is formed. However, the periodicity of this lamellar phase is substantially longer than observed for the LPP in stratum corneum and in mixtures prepared from CER:CHOL:FFA (9, 10, 22-24). Particularly, in the case of the synthetic CERs, the CER:CHOL:FFA mixtures mimicking the lipid composition in stratum corneum form a LPP with a repeat distance of approximately 12.2 nm (24). This shows that the lipid arrangement in the 14.7 nm lamellar phase of the EOS:CHOL:FFA mixture is different from that in the LPP of the CER:CHOL:FFA mixtures. From this observation we conclude that EOS requires the presence of other CERs to form the LPP. Examining more closely the molecular organisation of this 14.7 nm lamellar phase might, however, provide useful information on the formation of the LPP, as the presence of EOS and CHOL is crucial for the formation of both lamellar phases.

As also noticed in previous studies (34, 35), the equilibration of the samples is a very important step to obtain lamellar phases with very long repeat distances. For example, in order to obtain the lamellar phase in our equimolar EOS:CHOL:FFA mixture it was required to equilibrate the sample close to the temperature region at which the melting occurs, that is at 80ºC. An equilibration temperature of 70ºC, which is below the melting

temperature of the sample, does not lead to the formation of the lamellar phase with a very long periodicity (not shown), but results in a diffraction pattern with an undefined lipid phase behaviour indicating an improper mixing of the various compounds. Using a longer equilibration time at elevated temperatures, does not affect the formation of the lamellar phases.

### Lipid organisation of the EOS:CHOL:FFA mixtures

Considering the lamellar phase with the long repeat distance varying between 14.4 and 15.1 nm, we noticed exceptional phase behaviour in several aspects. In the discussion below we will refer to this phase as the 14.7 nm lamellar phase, despite the small variations in repeat distance. The combined information obtained with FTIR spectroscopy and X-ray diffraction will be used to provide a molecular arrangement of this lamellar phase. First we will discuss point by point the exceptional phase behaviour of this phase.

a. A slight deviation in CHOL levels from equimolar in the EOS:CHOL:FFA mixture reduces strongly the formation of the 14.7 nm lamellar phase. A deviation in FFA levels proved to be less critical since a small deviation of the FFA molar ratio varying between 1:1:0.8 EOS:CHOL:FFA and 1:1:1.2 EOS:CHOL:FFA still results in the formation of the 14.7 nm lamellar phase.

b. A certain degree of FFA chain length distribution is important for the formation of the 14.7 nm lamellar phase. When reducing the number of FFA components from 7 to 3, it is still possible to form the 14.7 nm lamellar phase, but only when using FFA chain lengths of at least 20 C atoms. This demonstrates that long chain fatty acids are required for the formation of the 14.7 nm lamellar phase.

c. When comparing the thermotropic behaviour in the symmetric stretching absorption of EOS:CHOL and EOS:CHOL:FFA samples, we can conclude that the addition of FFA to the EOS:CHOL mixture results in a higher conformational ordering and a larger temperature range for the melting transition, as the melting starts already at lower temperatures.

d. Substituting FFA by DFFA resulted in several remarkable and apparently contrasting observations. Compared to the DFFA spectrum, the contours of

the $CD_2$ scissoring frequencies of EOS:CHOL:DFFA are asymmetric and the degree of splitting is clearly reduced, demonstrating that the domain sizes of the deuterated chains in the equimolar EOS:CHOL:DFFA are smaller than the domain sizes in a DFFA mixture only (36). From these observations it is obvious that the short range coupling between DFFA in the EOS:CHOL:DFFA mixture is reduced as compared to a DFFA mixture. Thus, a certain fraction of the hydrocarbon chains of EOS is participating in the same lattice as the DFFA. This is very similar to the observations made in mixtures of CER:CHOL:FFA forming the LPP, reported recently (26, 37).

e. However, the thermotropic response of the conformational disordering shows a very remarkable behaviour: the conformational disordering of the DFFA occurs in a temperature region which is approximately 10ºC lower than the temperature region at which the major population of the hydrocarbon chains of EOS transforms from an ordered to a disordered phase. This clearly shows that although a subpopulation of hydrocarbon chains of EOS and DFFA are participating in the same orthorhombic lattice, a large fraction of the EOS and DFFA chains is not located in the same lattice and forms a separate domain.

f. The X-ray diffraction studies revealed that besides the presence of low levels of crystalline CHOL, only a 14.7 nm lamellar phase is formed in the equimolar EOS:CHOL:FFA mixture.

From this and from the observations made above, we can conclude that the 14.7 nm unit cell contains two types of domains: one in which FFA and EOS participate in an orthorhombic lattice and one in which the hydrocarbon chains of EOS and FFA do not mix.

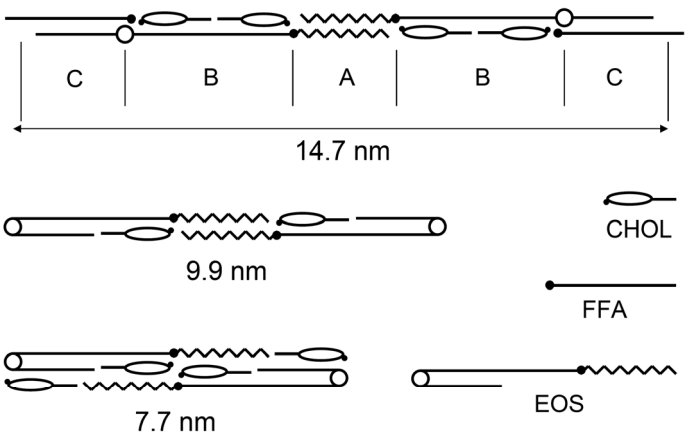


**Figure 6: Suggested molecular arrangement for the very long periodicity phase in EOS:CHOL:FFA mixtures and for the two lamellar phases present in EOS:CHOL mixtures.**

### Proposed molecular arrangement for the 14.7 nm lamellar phase

When combining all observations discussed above, a molecular arrangement for the 14.7 nm lamellar phase can be proposed. Such a molecular arrangement is provided in Figure 6. This arrangement shows three different lipid layers unequal in width. The different layers are referred to as layer A (central part), layer B (layer with ω-hydroxy fatty acid (C30) of EOS) and layer C (FFA containing layer). In the molecular arrangement in Figure 6 the length of the unit cell is determined by the two EOS molecules in linear arrangement, in which the linoleate moieties in the central part of the unit cell are interdigitating. When assuming a 0.127 nm length per C-C bonding, the total length of the unit cell calculated from the molecular structure of the two EOS molecules is 14.7 nm, which is in excellent agreement with the periodicity measured by x-ray diffraction. Furthermore, our measurements also revealed that two different domains are present in the unit cell of the 14.7 nm phase, most probably located in different lipid layers. This conclusion was drawn from the exceptional observation that

protonated and deuterated chains undergo an ordered-disordered transition in clearly different temperature ranges. Therefore, in our proposed arrangement the FFA is located adjacent to the C18 sphingosine chain of EOS in layer C forming the orthorhombic lattice. Furthermore, the FFA and the C18 sphingosine chain are partly interdigitating. The domain in layer B with mainly ω-hydroxy fatty acid (C30) of EOS and CHOL is responsible for the high temperature order-disorder transition of around 75ºC. A higher transition temperature is expected as the very long ω-hydroxy fatty acid chain is involved in this transition. Then the question arises, why is the FFA not located adjacent to the EOS C30 chain in layer B? One argument is the large chain length difference between FFA and the C30 chain of approximately 6 to 10 C-atoms. Therefore, these chains do not fit in one lipid layer. In addition, this arrangement cannot explain the difference in temperature range at which the order-disorder transition occurs for the protonated and deuterated chains, as the C18 sphingosine chains are not expected to undergo an ordered-disordered phase transition at a higher temperature than the chains of the FFA. Another possible location for FFA is adjacent to the linoleate moiety of EOS in layer A. However, the linoleate has a high conformational disordering already at 20ºC and therefore no short-range coupling between FFA and the linoleate moiety is possible and thus no orthorhombic phase can be formed after addition of the FFA. The final possibility to discuss is an arrangement of the FFA and CHOL in layer C, while the sphingosine chain would be located adjacent to the ω-hydroxy fatty acid chain of EOS. In this case a forked arrangement of the EOS is obtained. However, in this arrangement the reduction in splitting when substituting the FFA by DFFA cannot be explained as the CER and FFA chains are located in different layers.

Then the remaining question is whether the proposed arrangement in Figure 6 fulfils the requirement of an approximately equimolar ratio in the EOS:CHOL:FFA mixture. If indeed EOS is in a linear arrangement, the FFA and EOS might have an interfacial area of approximately 0.20 $nm^2$, similarly to that of sphingosine monolayers (38). In contrast, the interfacial area per

CHOL molecule is approximately 0.38-0.40 $nm^2$ (39), which is almost twice that of linearly arranged EOS and FFA. Perhaps the orientation of the bulky ring moiety of CHOL is perpendicular to the plane of drawing and a second EOS molecule is located on top of the EOS in the drawing, adjacent to the same CHOL molecule. In this way an equimolar ratio of EOS:CHOL:FFA is indeed achieved.

## A suggested molecular arrangement for the lamellar phases in EOS:CHOL mixtures

In the EOS:CHOL mixtures two lamellar phases are observed. At relatively low CHOL levels the repeat distance is approximately 9.8 nm, while at high CHOL levels the 7.7 nm lamellar phase is predominantly present. In the proposed molecular arrangement for the 14.7 nm lamellar phase, the hydroxyl group of the CHOL molecule is located close to the ester bond linking the C30 acyl with the linoleate moiety of EOS. Possibly, a hydrogen bonding between the hydroxyl group of CHOL and the ester group of EOS is stabilizing this arrangement. Furthermore, the linoleate moiety is fully interdigitating. When assuming a 0.127 nm distance per C-C bonding, this arrangement results in a calculated periodicity of 9.9 nm, which is very close to the experimental repeat distance. In this case we cannot distinguish between a forked or a linear arrangement of the EOS, both arrangements are possible. In the figure a forked arrangement is shown. When increasing the CHOL levels in the EOS:CHOL mixture a phase with a shorter repeat distance is found. An arrangement for this shorter repeat period accounting for the higher levels in CHOL content is also proposed in Figure 6. Again, the hydrogen bonding between the hydroxyl group of CHOL and the ester linkage in the EOS molecule might be the important factor that stabilizes the structure. Also, the calculated repeat distance is about 7.7 nm, which again matches with the measured repeat distance for this lamellar phase.

### A comparison between the LPP and the 14.7 nm lamellar phase

When we compare the phase behaviour of the LPP with that of the 14.7 nm lamellar phase, some important differences are observed. Most strikingly the 14.7 nm lamellar phase can only be formed when the EOS:CHOL molar ratio in the EOS:CHOL:FFA mixture is close to equimolar, while the LPP can be formed over a wide range of CER:CHOL molar ratios. In case of human CER e.g., the LPP is already formed at a CER:CHOL molar ratio of 1:0.2 in the absence of FFA (40). This means that FFA is not required to form the LPP, while CER and CHOL can replace each other to a certain extent in the LPP. For maintaining the barrier function of the skin, this is a very important observation, as even when dealing with substantial deviations in CER:CHOL molar ratios, the LPP, which is considered to be crucial for the skin barrier function, is still formed in the stratum corneum. In other words, the lipid phase behaviour is not very sensitive to changes in the lipid composition. As far as the role of FFA is concerned, it plays a prominent role in the formation of the orthorhombic lateral packing (41). In contrast to the LPP, in case of the 14.7 nm lamellar phase our results suggest that the three lipid classes including FFA are required to form the 14.7 nm lamellar phase.

Finally, the question rises whether EOS is arranged in the LPP in a linear or in a forked configuration. In the present study we propose a linear arrangement for the EOS in the lamellar phase with a periodicity of around 14.7 nm, as this results in the required mixing of the hydrocarbon chains of FFA and EOS. For other CER mixtures, a linear arrangement is also suggested for AP with a fatty acid chain of 18 carbon atoms (42, 43). However, whether the arrangement of EOS in the LPP is linear or forked remains to be elucidated as very small changes in the environment such as a distribution in chain length of the FFA and CER molecules or a variation in head-group architecture may affect this arrangement. In this paper we reported the phase behaviour of mixtures containing EOS, CHOL and FFA. Our studies showed that the two complimentary methods of X-ray diffraction and FTIR are excellent tools to provide detailed information on the 14.7 nm lamellar phase.

**Acknowledgments**

We thank the company Cosmoferm B.V. (Evonik) for the provision of the ceramide EOS and the Netherlands Organization for Scientific Research (NWO) for the provision of beam time at the ESRF. Furthermore we thank the personnel at the DUBBLE beam line 26 at the ESRF for their support with the x-ray measurements, as well as the group of crystallography at the University of Amsterdam for additional x-ray measurements.

## References


1. Motta, S., M. Monti, S. Sesana, R. Caputo, S. Carelli, and R. Ghidoni. 1993. Ceramide composition of the psoriatic scale. Biochim Biophys Acta 1182:147-151.
2. Proksch, E., J. M. Brandner, and J. M. Jensen. 2008. The skin: an indispensable barrier. Exp Dermatol 17:1063-1072.
3. Nemes, Z., and P. M. Steinert. 1999. Bricks and mortar of the epidermal barrier. Exp Mol Med 31:5-19.
4. Bodde, H. E., M. A. M. Kruithof, J. Brussee, and H. K. Koerten. 1989. Visualisation of normal and enhanced $HgCl_2$ transport through human skin in vitro. Int J Pharm 53:13-24.
5. Talreja, P., N. K. Kleene, W. L. Pickens, T. F. Wang, and G. B. Kasting. 2001. Visualization of the lipid barrier and measurement of lipid pathlength in human stratum corneum. AAPS PharmSci 3:E13.
6. Ponec, M., A. Weerheim, J. Kempenaar, A. M. Mommaas, and D. H. Nugteren. 1988. Lipid composition of cultured human keratinocytes in relation to their differentiation. J Lipid Res 29:949-961.
7. Wertz, P. W., and D. T. Downing. 1983. Ceramides of pig epidermis: structure determination. J Lipid Res 24:759-765.
8. Masukawa, Y., H. Narita, E. Shimizu, N. Kondo, Y. Sugai, T. Oba, R. Homma, J. Ishikawa, Y. Takagi, T. Kitahara, Y. Takema, and K. Kita. 2008. Characterization of overall ceramide species in human stratum corneum. J Lipid Res 49:1466-1476.
9. White, S. H., D. Mirejovsky, and G. I. King. 1988. Structure of lamellar lipid domains and corneocyte envelopes of murine stratum corneum. An X-ray diffraction study. Biochemistry 27:3725-3732.
10. Bouwstra, J. A., G. S. Gooris, J. A. van der Spek, and W. Bras. 1991. Structural investigations of human stratum corneum by small-angle X-ray scattering. J Invest Dermatol 97:1005-1012.
11. Hatta, I., N. Ohta, K. Inoue, and N. Yagi. 2006. Coexistence of two domains in intercellular lipid matrix of stratum corneum. Biochim Biophys Acta 1758:1830-1836.
12. Cornwell, P. A., B. W. Barry, C. P. Stoddart, and J. A. Bouwstra. 1994. Wide-angle X-ray diffraction of human stratum corneum: effects of hydration and terpene enhancer treatment. J Pharm Pharmacol 46:938-950.
13. Ohta, N., S. Ban, H. Tanaka, S. Nakata, and I. Hatta. 2003. Swelling of intercellular lipid lamellar structure with short repeat distance in hairless mouse stratum corneum as studied by X-ray diffraction. Chem Phys Lipids 123:1-8.
14. Fujii, M., Y. Takeda, M. Yoshida, N. Utoguchi, M. Matsumoto, and Y. Watanabe. 2003. Comparison of skin permeation enhancement by 3-l-menthoxypropane-1,2-diol and l-menthol: the permeation of indomethacin and antipyrine through Yucatan micropig skin and

changes in infrared spectra and X-ray diffraction patterns of stratum corneum. Int J Pharm 258:217-223.
15. Garson, J. C., J. Doucet, J. L. Leveque, and G. Tsoucaris. 1991. Oriented structure in human stratum corneum revealed by X-ray diffraction. J Invest Dermatol 96:43-49.
16. Bommannan, D., R. O. Potts, and R. H. Guy. 1990. Examination of stratum corneum barrier function in vivo by infrared spectroscopy. J Invest Dermatol 95:403-408.
17. Bouwstra, J. A., G. S. Gooris, J. A. van der Spek, S. Lavrijsen, and W. Bras. 1994. The lipid and protein structure of mouse stratum corneum: a wide and small angle diffraction study. Biochim Biophys Acta 1212:183-192.
18. Pilgram, G. S., A. M. Engelsma-van Pelt, J. A. Bouwstra, and H. K. Koerten. 1999. Electron diffraction provides new information on human stratum corneum lipid organization studied in relation to depth and temperature. J Invest Dermatol 113:403-409.
19. Boncheva, M., F. Damien, and V. Normand. 2008. Molecular organization of the lipid matrix in intact Stratum corneum using ATR-FTIR spectroscopy. Biochim Biophys Acta 1778:1344-1355.
20. Ponec, M., A. Weerheim, P. Lankhorst, and P. Wertz. 2003. New acylceramide in native and reconstructed epidermis. J Invest Dermatol 120:581-588.
21. Wertz, P. 1991. In Physiology, Biochemistry and Molecular Biology of the Skin. L. A. Goldsmith, editor. Oxford University Press, Oxford. 205-235.
22. Bouwstra, J. A., G. S. Gooris, K. Cheng, A. Weerheim, W. Bras, and M. Ponec. 1996. Phase behavior of isolated skin lipids. J Lipid Res 37:999-1011.
23. Bouwstra, J. A., G. S. Gooris, F. E. Dubbelaar, and M. Ponec. 2002. Phase behavior of stratum corneum lipid mixtures based on human ceramides: the role of natural and synthetic ceramide 1. J Invest Dermatol 118:606-617.
24. de Jager, M. W., G. S. Gooris, M. Ponec, and J. A. Bouwstra. 2005. Lipid mixtures prepared with well-defined synthetic ceramides closely mimic the unique stratum corneum lipid phase behavior. J Lipid Res 46:2649-2656.
25. McIntosh, T. J. 2003. Organization of skin stratum corneum extracellular lamellae: diffraction evidence for asymmetric distribution of cholesterol. Biophys J 85:1675-1681.
26. Janssens, M., G. S. Gooris, and J. A. Bouwstra. 2009. Infrared spectroscopy studies of mixtures prepared with synthetic ceramides varying in head group architecture: coexistence of liquid and crystalline phases. Biochim Biophys Acta 1788:732-742.
27. Brief, E., S. Kwak, J. T. Cheng, N. Kitson, J. Thewalt, and M. Lafleur. 2009. Phase behavior of an equimolar mixture of N-palmitoyl-D-erythro-sphingosine, cholesterol, and palmitic acid, a mixture with optimized hydrophobic matching. Langmuir 25:7523-7532.

28. Chen, X., S. Kwak, M. Lafleur, M. Bloom, N. Kitson, and J. Thewalt. 2007. Fatty acids influence "solid" phase formation in models of stratum corneum intercellular membranes. Langmuir 23:5548-5556.
29. Moore, D. J., M. E. Rerek, and R. Mendelsohn. 1997. Lipid domains and orthorhombic phases in model stratum corneum: evidence from Fourier transform infrared spectroscopy studies. Biochem Biophys Res Commun 231:797-801.
30. Neubert, R., W. Rettig, S. Wartewig, M. Wegener, and A. Wienhold. 1997. Structure of stratum corneum lipids characterized by FT-Raman spectroscopy and DSC. II. Mixtures of ceramides and saturated fatty acids. Chem Phys Lipids 89:3-14.
31. Bouwstra, J. A., J. Thewalt, G. S. Gooris, and N. Kitson. 1997. A model membrane approach to the epidermal permeability barrier: an X-ray diffraction study. Biochemistry 36:7717-7725.
32. Wertz, P. 1991. Epidermal lipids. In Physiology, Biochemistry and Molecular Biology of the Skin. L. A. Goldsmith, editor. Oxford University Press, Oxford. 205-235.
33. Small, D. M. 1986. The Physical Chemistry of Lipids. In Handbook of Lipid Research. D. J. Hanahan, editor. Plenum Press, New York.
34. de Jager, M. W., G. S. Gooris, I. P. Dolbnya, W. Bras, M. Ponec, and J. A. Bouwstra. 2004. Novel lipid mixtures based on synthetic ceramides reproduce the unique stratum corneum lipid organization. J Lipid Res 45:923-932.
35. Groen, D., G. S. Gooris, M. Ponec, and J. A. Bouwstra. 2008. Two new methods for preparing a unique stratum corneum substitute. Biochim Biophys Acta 1778:2421-2429.
36. Snyder, R. G., M. C. Goh, V. J. P. Srivatsavoy, H. L. Strauss, and D. L. Dorset. 1992. Measurement of the growth kinetics of microdomains in binary n-alkane solid solutions by infrared spectroscopy. J Phys Chem 96:10008-10019.
37. Gooris, G. S., and J. A. Bouwstra. 2007. Infrared spectroscopic study of stratum corneum model membranes prepared from human ceramides, cholesterol, and fatty acids. Biophys J 92:2785-2795.
38. Vaknin, D. 2003. Structure-function relations in self-assembled C18- and C20-sphingosines monolayers at gas/water interfaces. J Am Chem Soc 125:1313-1318.
39. Scheffer, L., I. Solomonov, M. J. Weygand, K. Kjaer, L. Leiserowitz, and L. Addadi. 2005. Structure of cholesterol/ceramide monolayer mixtures: implications to the molecular organization of lipid rafts. Biophys J 88:3381-3391.
40. Bouwstra, J. A., G. S. Gooris, F. E. Dubbelaar, and M. Ponec. 2001. Phase behavior of lipid mixtures based on human ceramides: coexistence of crystalline and liquid phases. J Lipid Res 42:1759-1770.
41. Bouwstra, J. A., G. S. Gooris, F. E. Dubbelaar, A. M. Weerheim, and M. Ponec. 1998. pH, cholesterol sulfate, and fatty acids affect the stratum corneum lipid organization. J Investig Dermatol Symp Proc 3:69-74.

42. Kiselev, M. A., N. Y. Ryabova, A. M. Balagurov, S. Dante, T. Hauss, J. Zbytovska, S. Wartewig, and R. H. Neubert. 2005. New insights into the structure and hydration of a stratum corneum lipid model membrane by neutron diffraction. Eur Biophys J 34:1030-1040.
43. Kessner, D., M. A. Kiselev, T. Hauss, S. Dante, S. Wartewig, and R. H. Neubert. 2008. Localisation of partially deuterated cholesterol in quaternary SC lipid model membranes: a neutron diffraction study. Eur Biophys J 37:1051-1057.